

ACCEPTED VERSION

Will Robertson, Ben Cazzolato, and Anthony Zander

Axial force between a thick coil and a cylindrical permanent magnet: optimising the geometry of an electromagnetic actuator

IEEE Transactions on Magnetics, 2012; 48(9):2479-2487

© 2012 IEEE. Personal use of this material is permitted. Permission from IEEE must be obtained for all other uses, in any current or future media, including reprinting/republishing this material for advertising or promotional purposes, creating new collective works, for resale or redistribution to servers or lists, or reuse of any copyrighted component of this work in other works.

Published version at: <http://dx.doi.org/10.1109/TMAG.2012.2194789>

PERMISSIONS

http://www.ieee.org/publications_standards/publications/rights/rights_policies.html

Authors and/or their employers shall have the right to post the accepted version of IEEE-copyrighted articles on their own personal servers or the servers of their institutions or employers without permission from IEEE, provided that the posted version includes a prominently displayed IEEE copyright notice (as shown in 8.1.9.B, above) and, when published, a full citation to the original IEEE publication, including a Digital Object Identifier (DOI). Authors shall not post the final, published versions of their articles.

3 July 2019

<http://hdl.handle.net/2440/73158>

Axial force between a thick coil and a cylindrical permanent magnet: optimising the geometry of an electromagnetic actuator.

Will Robertson, Ben Cazzolato, and Anthony Zander
School of Mechanical Engineering, The University of Adelaide, Australia

Abstract—In this paper a variety of analytical/integral methods are compared for calculating the axial force between a cylindrical magnet and a ‘thick’ solenoid that consists of many turns both radially and axially. Two newly developed techniques are introduced: one being numerical integration-based and the other completely analytical. These are compared to two other techniques, each shown to have various advantages in different contexts. One method in particular is introduced that is shown to be the most computationally efficient in the majority of actuator designs. This method is then used to optimise a typical ‘sleeve-type’ magnet–coil actuator based on the cost function of peak force, and it is shown that optimal values of wire thickness and magnet–coil geometry can be chosen based on desired coil impedance and magnet volume.

I. INTRODUCTION

The theory discussed in this paper is based around an integral expression that can be efficiently numerically implemented for calculating the axial force between a coaxial cylindrical magnet and a ‘thick’ solenoid that consists of many turns both radially and axially. This integral expression is compared against a variety of other methods.

The motivation for this work is the optimisation of the geometry of a coil–magnet actuator. We consider a ‘sleeve coil’ design in which a magnet of a certain volume moves inside a fixed coil of a certain impedance, and wish to optimise the geometric parameters to maximise the peak force of the actuator (although other metrics are also possible). Only the quasi-static force/displacement characteristics are considered; in other words, we neglect any inductance effects caused by the moving magnet, which could affect the high-frequency behaviour of the device.

When considering the literature for calculating the force between an electromagnetic coil and a cylindrical permanent magnet, expressions for both magnet–magnet and coil–coil forces are applicable since magnets and coils are electromagnetically equivalent according to the surface current density model of a permanent magnet. In early work in this field, Cooper et al. [1] presented an integral expression for calculating the force between two cylindrical magnets. Later, Furlani [2] published expressions for calculating the force between axially magnetised ring magnets, which with zero internal radius collapse to an expression for cylindrical magnets. However, this expression used an algorithm that requires discretising the magnet volumes into a large number of ‘magnetic charge’ point sources and summing the contri-

butions between each interacting pair; this is equivalent to a numerical integration in terms of computational efficiency.

More recently Babic et al. [3] and Ravaud et al. [4] presented closed form expressions for calculating the force between pairs of thin coils (in which there are many turns axially but the coil is modelled as having zero radial thickness). The expressions of Ravaud et al. [4] were simplified further in a recent publication by the present authors [5]. Babic et al. [6] has also published an equation for the axial force between a thin and thick coil under axial displacement, which is considered in more detail in this work.

A. Reproducibility

In order for the work in this paper to be easily reproduced and verified, the software implementation of the theory is available for public use at (<http://github.com/wspr/magcode>). Refer to the file ‘examples/Thick-Coil-Magnet-Forces.nb’ for the source of the graphs in this publication. While this file is written for the Mathematica programming language, the software available is written for both Matlab and Mathematica and contains numerical implementations for not just this work but also a variety of other permanent magnet calculations.

II. GEOMETRY

The system under investigation is shown in Figures 1 and 2. In this work there is no restriction on the size or geometry of the magnet or coil. To describe the geometry of the magnet–coil configuration, two aspect ratios are defined for the magnet and coil respectively. The ‘magnet ratio’ is given by the ratio between length and radius for the magnet, $\alpha = l_m/R_m$, and the ‘coil ratio’ similarly by the ratio between coil length and inner radius, $\beta = l_c/r_c$. The clearance (or gap) between the inner coil and magnet radii is denoted $r_g = r_c - R_m$.

The coil may have many turns in both axial and radial directions; denote N_z the number of turns axially and N_r the number of turns radially. Such a coil will have $N = N_z \times N_r$ turns in total, and assuming the turns are packed equally in both directions the coil will have a volume current density of $NI/[l_c[R_c - r_c]]$, where I is the current passing through the coil.

The permanent magnet is assumed to have a sufficiently large coercivity such that its magnetisation strength will not be affected by the magnetic field of the coil. The permanent magnet is also assumed to be homogeneous with a constant magnetisation strength B_r in the axial direction only.

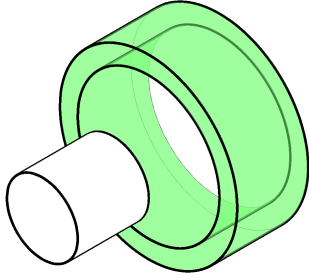


Fig. 1. Three-dimensional sketch of the system composed of a permanent magnet (unshaded, left) and thick coil (shaded, right). The magnet can be modelled as an equivalent cylindrical surface current density, and the coil as a volumetric current density.

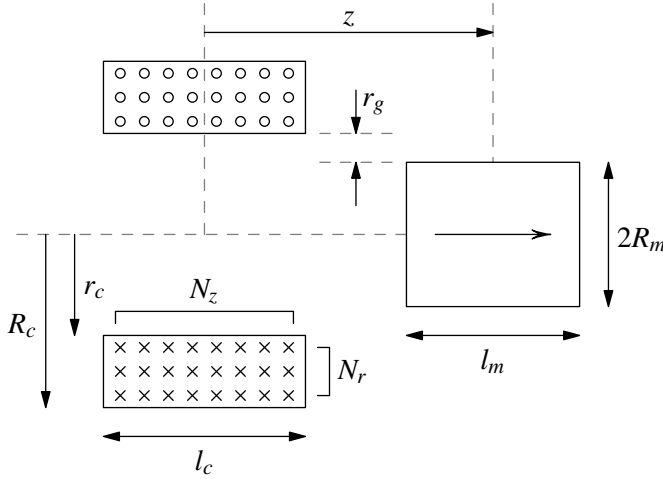


Fig. 2. Schematic of a 'sleeve coil' magnetic actuator. This geometry can be described in terms of magnet ratio $\alpha = l_m/R_m$ and coil ratio $\beta = l_c/r_c$.

III. THICK-COIL/MAGNET AXIAL FORCE METHODS

In this section we will discuss the theory for calculating the interaction force between the thick coil and permanent magnet configuration shown in Figure 1. In the first two force calculation methods, 'filament' and 'shell', the coil and/or magnet are modelled in terms of discrete elements (such as single-turn or thin coils) for which the interaction forces may be summed through superposition of each combination of elements. The final method uses a single integral expression to calculate the force, and two formulations and solutions for this integral are discussed.

A. The filament method

For two circular coaxial loops (i.e., a single turn of a solenoid) carrying currents I_1 and I_2 respectively, the axial force between them is given by [7, e.g.]

$$F_f(r_1, r_2, z) = \mu_0 I_1 I_2 z \sqrt{\frac{m}{4r_1 r_2}} \left[K(m) - \frac{m/2 - 1}{m - 1} E(m) \right] \quad (1)$$

$$m = \frac{4r_1 r_2}{[r_1 + r_2]^2 + z^2} \quad (2)$$

where r_1 and r_2 are the coil radii and z is the axial distance between them. The functions $K(m)$ and $E(m)$ are the complete

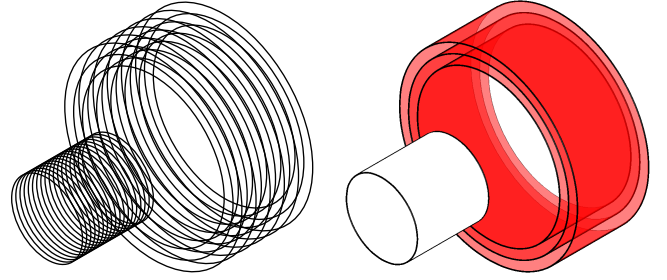


Fig. 3. The filament and shell models (left and right, respectively). In the filament model, the magnet and thick coil are modelled with individual current loops. In the shell model, the magnet is modelled as a cylindrical surface current density and the thick coil is modelled as a number of individual concentric surface current densities to represent multiple windings in the radial direction.

first and second elliptic integrals respectively with parameter m . These functions can also be referred to with notation $K(k)$ and $E(k)$ in terms of a modulus k , where $m = k^2$.

Using the 'filament method', equations (1) and (2) can be used to calculate the force between any arrangement of coaxial solenoids by representing each turn of the solenoid as a separate coil, and summing the forces through superposition for every pair-wise combination of coil interaction forces. Figure 3 shows such a filament model for the interaction between a thin coil (representing a permanent magnet) and a thick coil. Using this technique, the total force between them is given by

$$F_{z_1} = \sum_{n_m=1}^{N_m} \sum_{n_r=1}^{N_r} \sum_{n_z=1}^{N_z} F_f(r(n_r), R_m, z + L(n_m, n_z)), \quad (3)$$

$$r(n_r) = R_c + \frac{n_r - 1}{N_r - 1} [R_c - r_c], \quad (4)$$

$$L(n_m, n_z) = -\frac{1}{2} [l_m + l_c] + \frac{n_z - 1}{N_z - 1} l_c + \frac{n_m - 1}{N_m - 1} l_m, \quad (5)$$

where R_m is the magnet radius, r_c and R_c are the inner and outer coil radii, l_m and l_c are the magnet and coil lengths, z is the axial distance between their centres, N_r and N_z are the number of turns in the thick coil in the radial and axial direction, and N_m is the number of turns in the thin coil. The filament current $I_1 = I$ is the current in the thick coil. The arrangement of 'turns' used to model the permanent magnet is related to an equivalent surface current density with current per turn of $I_2 = B_r l_m / [N_m \mu_0]$ and permanent magnet strength B_r . The number of 'turns' N_m used to model the permanent magnet should be chosen to be sufficiently large such that the resultant force converges to a stable value.

B. The shell method

In the 'shell method', a thick solenoid and a magnet may be modelled by representing each radial layer of turns as a separate thin coil with surface current density $1/N_r$ the volume current density. The force between them is calculated

by summing the forces through superposition of the forces between each thin coil and the magnet.

$$F_{z2} = \frac{1}{N_r} \sum_{n_r=1}^{N_r} F_s(R_m, r(n_r), l_m, l_c, z) \quad (6)$$

$$r(n_r) = r_c + \frac{n_r - 1}{N_r - 1} [R_c - r_c] \quad (7)$$

where $F_s(R_m, r, l_m, l_c, z)$ is the force between a permanent magnet and a thin coil, given by [5]

$$F_s(R_m, r, l_m, l_c, z) = \frac{J_1 J_2}{2\mu_0} \sum_{e_1, e_2}^{\{1, -1\}^2} e_1 e_2 m_1 m_2 m_3 f_s. \quad (8)$$

$J_1 = B_r$ is the strength of the permanent magnet and $J_2 = \mu_0 N_z I / l_c$ where I is the current in the coil. The intermediate expression in equation (8) is given by

$$f_s = K(m_4) - \frac{1}{m_2} E(m_4) + \left[\frac{m_1^2}{m_2^2} - 1 \right] \Pi \left(\frac{m_4}{1 - m_2} \middle| m_4 \right), \quad (9)$$

with parameters

$$m_1 = z - \frac{1}{2} e_1 l_m - \frac{1}{2} e_2 l_c, \quad m_2 = \frac{[R_m - r]^2}{m_1^2} + 1, \quad (10)$$

$$m_3 = \sqrt{[R_m + r]^2 + m_1^2}, \quad m_4 = \frac{4R_m r}{m_3}. \quad (11)$$

The function $\Pi(n|m)$ is the complete elliptic integral of the third kind with parameter m .

C. An integral method

An integral expression for the force between a solenoid and magnet is derived using the theory of Furlani [8]. Here we have assumed that the solenoid can be modelled as a volume current density and the permanent magnet is modelled as a surface current density around its circumference. A solenoid with current volume density \mathbf{J} generates a magnetic field \mathbf{B} at a displacement \mathbf{d}_1 given by the integral over the coil volume V_c

$$\mathbf{B}(\mathbf{d}_1) = \frac{\mu_0}{4\pi} \int_{V_c} \frac{\mathbf{J}(\mathbf{d}_2) \times [\mathbf{d}_2 - \mathbf{d}_1]}{|\mathbf{d}_2 - \mathbf{d}_1|^3} dv_c, \quad (12)$$

where \mathbf{d}_2 is the distance vector to the differential coil volume dv_c . The force due to that field on a permanent magnet with magnetisation vector \mathbf{M} is given by the integral over the magnet surface S_m with normal vector $\hat{\mathbf{n}}$

$$\mathbf{F} = \oint_{S_m} [\mathbf{M} \times \hat{\mathbf{n}}] \times \mathbf{B}(\mathbf{d}_1) ds_m, \quad (13)$$

where \mathbf{d}_1 is the distance vector to the differential magnet surface ds_m . Following the magnetic field expression in polar coordinates shown by Ravaut et al. [9] and taking only the axial component of the force results, equation (13) is written in full as a function of axial displacement z as

$$F_{z3}(z) = \frac{B_r N I}{l_c [R_c - r_c]} \int_{-l_c/2}^{l_c/2} \int_0^{2\pi} \int_{r_c}^{R_c} \int_{z-l_m/2}^{z+l_m/2} \int_0^{2\pi} \frac{r_1 r_2 [r_2 - r_1] \cos(\phi_2 - \phi_1)}{|\mathbf{d}_2 - \mathbf{d}_1|^3} d\phi_1 dz_1 dr_2 d\phi_2 dz_2 \quad (14)$$

TABLE I
MAGNET-COIL PARAMETERS FOR VERIFYING THIN-COIL FORCE EQUATIONS (FIGURE 4). COIL THICKNESS IS USED FOR THE THICK COIL EQUATION ONLY.

Magnet radius	R_m	9mm
Magnet length	l_m	10mm
Magnet 'turns'	N_m	100
Magnet remanence	B_r	1T
Coil inner radius	r_c	10mm
Coil thickness	$R_c - r_c$	0.5mm
Coil length	l_c	20mm
Coil turns	N_z	40
Coil current	I	1A

where

$$|\mathbf{d}_2 - \mathbf{d}_1| = \sqrt{r_1^2 + r_2^2 - 2r_1 r_2 \cos(\phi_1 - \phi_2) + [z_2 - z_1]^2}. \quad (15)$$

Analytically integrating this equation in variables ϕ_1 , ϕ_2 , and z_1 yields

$$F_{z3} = \frac{B_r N I}{l_c [R_c - r_c]} \int_{-l_c/2}^{l_c/2} \int_{r_c}^{R_c} \sum_{e_1}^{\{1, -1\}} [e_1 m_6 f_{z3}] dr_2 dz_2, \quad (16)$$

where

$$f_{z3} = \left[1 - \frac{1}{2} m_5 \right] K(m_5) - E(m_5), \quad (17)$$

$$m_5 = \frac{4R_m r_2}{m_6^2}, \quad m_6^2 = [R_m + r_2]^2 + \left[z + \frac{1}{2} e_1 l_m - z_2 \right]^2. \quad (18)$$

Note that z_2 and r_2 in equation (18) are variables of integration.

Computing equation (16) using a numerical integration is an efficient means to calculate the axial force between a coaxial magnet and solenoid. This method is here referred to as the 'integral' method.

D. The integral method of Babic et al.

Babic et al. [6] presented a different solution for the integral of equation (14). Their solution consists of an entirely analytical component with one separate term requiring a single numerical integration. Corrected for a typographical error and rewritten slightly, their expression is shown in equation (30) in Appendix A and herein is referred to as the 'Babic' method.

E. Comparison of these methods

The filament model with a single radial turn ($N_r = 1$) can be used to verify the thin-coil magnet force, and an initial verification of the integral solution can be performed by comparing the thin-coil results for a thick-coil with coil thickness equal to the wire diameter. Force versus displacement calculations are performed with these three techniques (equations (3), (6) and (16)) using the physical parameters defined in Table I; these calculations are shown in Figure 4 and it can be seen that the three models produce comparable results. The results due to the filament model have a small discrepancy around the trough of the curve due to the discretisation of the magnet that this technique requires.

Having verified the filament, shell and integral methods for calculating the force between a thin coil and a magnet, we

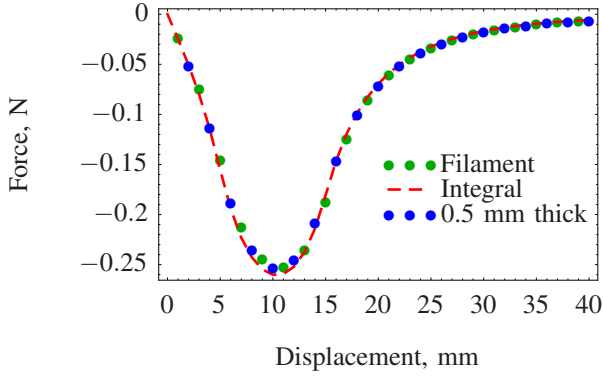


Fig. 4. Comparison between three methods for calculating the force versus axial displacement between a coaxial thin coil and magnet. For the filament and shell methods, the thin coil is modelled as having zero thickness. The thick coil force equation models the coil as a volumetric current density in this case with a radial thickness equal to the wire diameter.

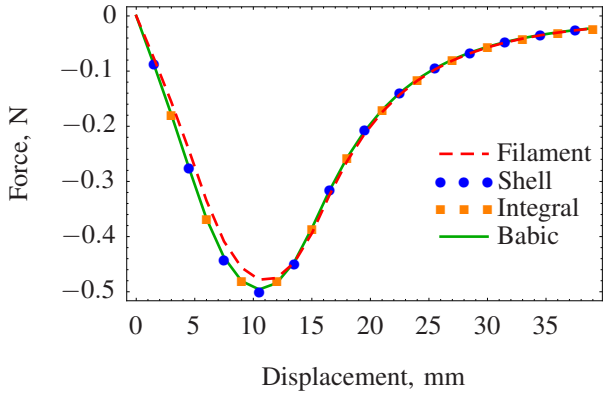


Fig. 5. Comparison between four methods for calculating the force versus axial displacement between a coaxial thick coil and magnet. The discretisation of the filament method incurs a small deviation from the expected results.

wish to now perform a similar comparison for calculating the force for a thick coil instead. A similar set of calculations are performed, including Babcic et al.'s integral approach (equation (30)), using the same set of parameters as in Table I except with a thick coil instead with a thickness $R_c - r_c = 5$ mm with $N_z = 20$ turns in the axial direction and $N_r = 5$ turns in the radial direction. The force versus displacement results for the thick coil/magnet calculations are shown in Figure 5, and again the four techniques compare closely to one another. In particular, the equation by Babcic et al. [6] produces consistent results with the integral expression introduced in this work. The discrepancy due to the discretisation of the filament model is larger here than for the results of Figure 4.

The four methods compared in Figure 5 all use different algorithms, and their execution speed varies significantly as a result. The shell method is more efficient than the filament method, since its execution time is linear with the number of radial layers of turns N_r due to a single summation term. The filament method is the slowest to execute of the four methods, as it has computation time proportional to $N_z \times N_r \times N_m$, which is approximately cubic with the number of turns in total.

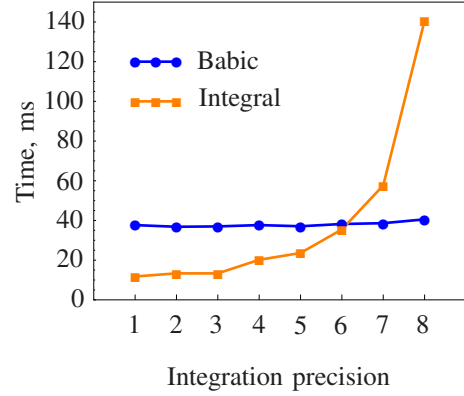


Fig. 6. Illustrative computation times for evaluating the results shown in Table II. Integration precision refers to the minimum number of accurate significant figures.

Of the two latter methods, for calculations requiring less stringent accuracy (say, to four significant figures precision) it is more efficient to use the ‘integral’ method (equation (16)) rather than the ‘Babcic’ method (equation (30)) due to the mathematical complexity of the latter, despite it requiring a lesser amount of numerical integration. This is illustrated in Figure 6, in which it can be seen that increasing the integration precision when performing calculations using Mathematica causes the time for numerical evaluation of the integral to increase exponentially, whereas the ‘Babcic’ method has a constant execution speed as its single term requiring numerical integration is only a small component of the overall equation. Nonetheless, as shown in the numerical results (Table II), the integral solution will generally produce results to a sufficient level of accuracy even with low integration accuracy thresholds and will therefore may be the preferred solution to evaluate in some cases, such as for optimisation studies.

In contrast, the shell method is much more efficient than either of the integral methods; it executes faster than the Babcic method by up to two orders of magnitude. In comparison to the 40ms time shown in Figure 6, the shell method executes in around 0.26ms per radial turn with a result differing by 0.0125% from the most accurate of Table II. The large improvement in execution speed of the shell method is due to the mathematical simplicity of its solution which does not require numerical integration. Despite the presence of small variations in the results due to the discretisation of the algorithm, this method will be significantly faster with comparable results than the other techniques discussed in this section for analysing thick coils with up to around 10^2 number of radial turns.

While the computational times given in this section are specific to the platform used to perform the calculations, their relative differences should be comparable across different computers and numerical implementations.

IV. OPTIMISATION OF A SLEEVE COIL MAGNETIC ACTUATOR

In the previous sections, we have presented equations for calculating coil forces with arbitrary examples for verification.

TABLE II
NUMERICAL OUTPUT WITH INCREASING INTEGRATION PRECISION.
GREYED DIGITS INDICATE INACCURACY IN THE RESULT AFTER
ROUNDING TO THAT MANY SIGNIFICANT FIGURES.

Prec.	Method	
	Babic, eq. (30)	Integral, eq. (16)
1	2.4544407879895993	2.4744006907978187
2	2.4544407879895993	2.4548594892044457
3	2.4544407879895993	2.4548594892044457
4	2.4544438306124783	2.4544392729491915
5	2.4544438306124783	2.4544410458278520
6	2.4544438296675000	2.4544437864466280
7	2.4544438300939190	2.4544438175568843
8	2.4544438300903315	2.454443829997147
9	2.4544438300903315	2.4544438301061358
10	2.4544438300903230	2.4544438300904050

These equations can be used for design optimisation for magnetic actuator design; for example, to choose geometric parameters for an inertial shaker to maximise the peak force or to maximise the stroke length. In this section, a common ‘sleeve coil’ configuration is investigated in which a cylindrical magnet moves axially within a hollow coil, such that the inner coil radius is greater than the magnet radius; $r_c > R_m$. A schematic of this system is shown in Figure 2.

A. Relationship between coil impedance and outer diameter

When attempting to optimise the force output of a coil/magnet design, it is important to carefully consider the parameters to be varied so that comparisons between different cases are fair. In the theory developed in Section III, the force is calculated using coils of a given current density and coil thickness. When designing a coil, however, it is instead more applicable to fix the coil resistance and wire thickness and calculate the number of turns and outer coil radius from these values. In this way, comparisons between different geometries will be indicative of force for some fixed electrical input power as each coil variation will draw the same amount of current for a given driving voltage.

The resistance of the coil R directly infers the length of the wire winding, l_w , through the relation

$$l_w = Ra_w/\rho, \quad (19)$$

for wire of cross sectional area a_w (assumed here as having circular cross section $a_w = \pi [\frac{1}{2}d_w]^2$), and resistivity ρ .

The fixed parameters of the coil are driving voltage, resistance, wire thickness and material, which in turn fix the total length of wire. Given a total length of wire, it is possible to derive a relation between the coil length, l_c , and the coil radii, r_c and R_c . Assuming that each turn of wire sits directly above or adjacent to its neighbours, an approximate expression for the total wire length is given by

$$l_w = N_z \sum_{n=0}^{N_r-1} 2\pi \left[r_c + d_w \left[n + \frac{1}{2} \right] \right] = 2\pi N_r N_z \left[r_c + \frac{1}{2} N_r d_w \right], \quad (20)$$

where $N_r = [R_c - r_c]/d_w$ and $N_z = l_c/d_w$ are the number of turns in the axial and radial directions respectively. While this

relationship does not model any wire coating or the packing effect of how tightly-wound coils will sit, this equation is simple and allows some conservatism in the quality of the construction of the electromagnet.

Therefore, an expression for the outer radius of the coil for a coil of fixed inner radius and fixed total wire length is

$$R_c = \sqrt{\frac{l_w d_w^2}{\pi l_c} + r_c^2}. \quad (21)$$

B. Notation

From Section III, the axial force versus displacement for a coil/magnet system can be expressed as a function of its gross geometric parameters (defined in Figure 1) as

$$F_z(B_r, I, N_z, N_r, R_m, l_m, r_c, R_c, l_c | z), \quad (22)$$

with electromagnetic parameters (B_r , I , N_z , N_r) defined previously and F_z calculated with any of the filament, shell, or integral methods (equations (3), (6), (16) and (30), resp.).

The magnet radius R_m can be expressed in terms of the magnet ratio α and magnet volume V_m with

$$R_m = \left[\frac{V_m}{\pi \alpha} \right]^{1/3}, \quad (23)$$

from which the magnet length $l_m = \alpha R_m$, coil inner radius $r_c = R_m + r_g$, and coil length $l_c = \beta r_c$ are inferred directly from the geometric ratios and clearance between the coil and magnet r_g .

As discussed in Section IV-A, the outer coil radius R_c and the coil turns N_z and N_r can be calculated from the coil resistance R , wire diameter d_w and wire resistivity ρ . Therefore, the force function of equation (22) can be expressed in terms of the following different set of parameters which are more useful for design optimisation:

$$F_z(B_r, I, \rho, V_m, R, d_w, \alpha, \beta, r_g | z). \quad (24)$$

Of these parameters, the magnet strength is set to be $B_r = 1$ T, the radial clearance is fixed at $r_g = r_c - R_m = 0.5$ mm, and the resistivity of copper of $\rho = 1.7 \times 10^{-8} \Omega \text{m}$ is used. Initially the normalised force per unit current \hat{F}_z is considered, which is calculated by evaluating the force for a current of $I = 1$ A. Removing these fixed parameters from equation (24) produces

$$\hat{F}_z(V_m, R, d_w, \alpha, \beta | z). \quad (25)$$

In the sections to come, the coil-magnet force F_z will be discussed as a function of magnet volume V_m , coil resistance R , wire diameter d_w , magnet ratio α , coil ratio β , and axial displacement z . The goal of the analysis will be to derive optimum values for certain of these parameters.

At the outset it is assumed that increasing the magnet volume V_m will result in greater forces since there will be a greater amount of magnetic energy in the system; this is not then a parameter to be varied but instead to be selected as necessary.

C. Optimisation of magnet and coil geometry

To perform the optimisation of magnet and coil geometries, the shell method, equation (6), is used to calculate the force as a function of displacement with varying magnet and coil ratios.

For sake of example, a wire diameter $d_w = 1$ mm was selected to produce the initial results; wire diameter is varied in Section IV-D. The volume of magnetic material is held constant at $V_m = [20\text{mm}]^3$ and the coil impedance at $R = 4\Omega$. Therefore the normalised force per unit current is calculated for this case as

$$\hat{F}_z(\alpha, \beta|z) = \hat{F}_z([20\text{mm}]^3, 4\Omega, 1\text{mm}, \alpha, \beta|z). \quad (26)$$

The effects on the force–displacement characteristic of equation (26) of varying the magnet ratio α and coil ratio β independently are shown respectively in Figure 7. For each it can be seen that the peak force and the shape of the curve varies quite significantly as the geometry of the magnet and coil changes. It can also be seen that an optimal α and β could be chosen to satisfy a particular cost function such as peak force, integral of force over displacement, displacement over which at least 95% of the peak force is achieved, linearity over a certain displacement range, and so on, according to the requirements of the actuator being designed. For simplicity, in the examples to follow we shall consider peak force as the metric to be maximised but the methodology for design optimisation holds regardless of the cost function.

The magnet and coil ratios α and β were considered over a range from 0.1 to 10 and the normalised peak force over displacement calculated as a function of these two varying parameters. The normalised peak force was calculated as

$$\hat{F}_{\text{peak}}(V_m, R, d_w, \alpha, \beta) = \max_z \left\{ \hat{F}_z(V_m, R, d_w, \alpha, \beta|z) \right\}, \quad (27)$$

where magnet volume V_m , coil resistance R , and wire diameter d_w were fixed as described earlier.

Figure 8 shows an example of the surface produced after evaluating the normalised peak force with equation (27) over a discretisation of the magnet and coil ratio ranges. This surface can be seen to be concave, and therefore a single value for α and β can be chosen to maximise the normalised peak force for a given magnet volume, coil impedance, and wire diameter.

D. Optimisation of wire diameter

In Section IV-C, the peak force results were normalised against coil current and the effect of wire diameter has not been taken into account. However, the wire diameter is a particularly important parameter, as it directly infers the length of wire to be used but more importantly restricts the current carrying capacity of the coil. A larger diameter wire will produce a lower resistance per unit length, and hence for a given input impedance a longer wire length in total. Depending on the geometry of the coil, having a longer wire length could cause the coil to become unnecessarily thick, moving magnetic energy away from where it is required, which is as close as possible to the permanent magnet. Having shown a method by which an optimal magnet and coil geometry can be chosen

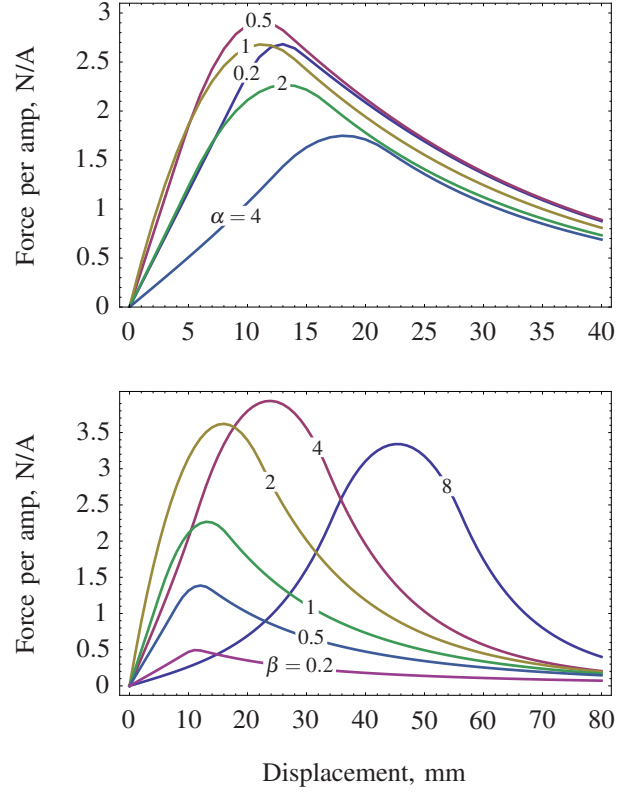


Fig. 7. Normalised force \hat{F}_z versus displacement calculations for two cases: firstly, varying magnet ratio α for a fixed coil ratio $\beta = 1$, and secondly varying coil ratio β for a fixed magnet ratio $\alpha = 2$.

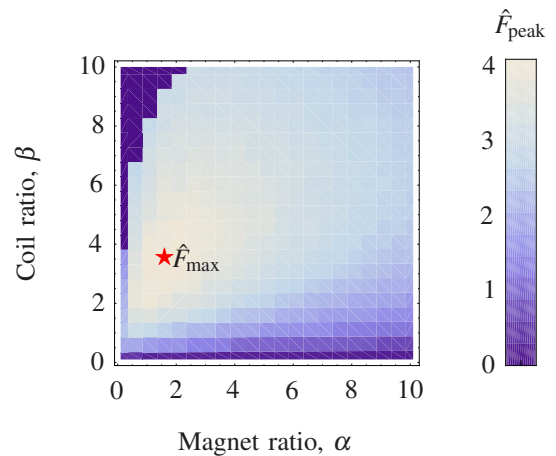


Fig. 8. Peak normalised force \hat{F}_{peak} as magnet and coil ratios α and β are varied over a 20×20 discrete grid for a specific wire diameter, coil impedance, and magnet volume. Maximum normalised peak force is indicated with a star.

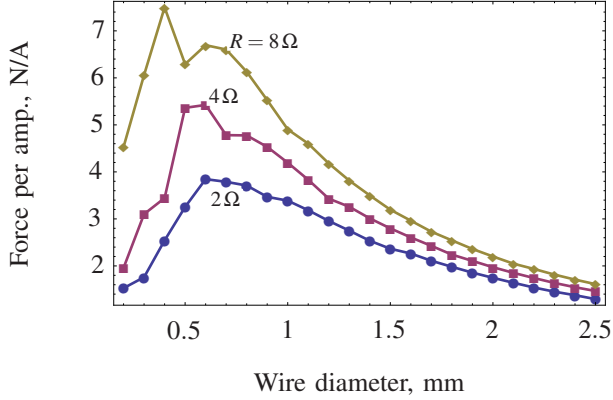


Fig. 9. Maximum normalised force per ampere of current, optimised by magnet and coil geometry as a function of wire diameter. Results are shown for three values of coil impedance while the magnet volume is fixed at $V_m = (20\text{mm})^3$.

(e.g., as shown in Figure 8) it is now possible to introduce the wire diameter as a variable parameter, which will allow an optimal wire diameter to be chosen.

First consider the case of optimising the normalised peak force per unit of current over magnet and coil ratios and a range of wire diameters using the equation

$$\hat{F}_{\max}(V_m, R, d_w) = \max_{\alpha, \beta} \left\{ \hat{F}_{\text{peak}}(V_m, R, d_w, \alpha, \beta) \right\}. \quad (28)$$

Rather than gridding the parameter space for α and β into discrete values as in Figure 8, which has limited precision, this optimisation was performed using a two-dimensional local maximum search function (Mathematica's `FindMaximum`). The results from evaluating equation (28) as a function of wire diameter over a range of coil resistances is shown in Figure 9. As the wire diameter increases, the resistance per unit length decreases and a larger coil is required; past a certain point, this decreases the amount of force per unit current that the coil can achieve.

Figure 9 is noisy at small wire diameters due to quantisation errors in calculating the number of turns of the coil. When calculating the outer radius of the coil with equation (21), a non-integer number of radial turns is required to achieve an exact wire length, and discrepancies result as the number of radial turns is quantised. These errors are greater at lower wire diameters as each individual coil turn contributes a greater proportional of the total coil resistance.

E. Consideration of maximum current rating

As the wire diameter increases, the amount of force per unit of current decreases. However, as the wire diameter increases the maximum current rating increases as well; larger wire diameters can be driven with a larger input voltage.

There is a general relationship relating wire diameter and its maximum current rating [10], denoted $I_{\max}(d_w)$ and shown in Figure 10; note that although this relationship is conservative it does not take into account factors such as thermal loading due to tightly-wound coils or high-frequency current oscillations.

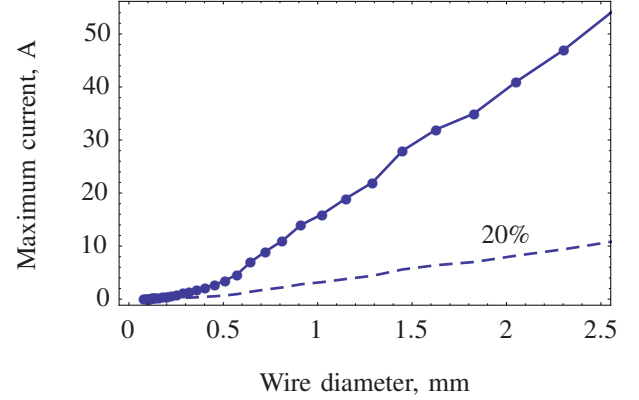


Fig. 10. Typical values for maximum current rating for copper wire of varying diameter [10, adapted], and the same data with a 20% safety factor.

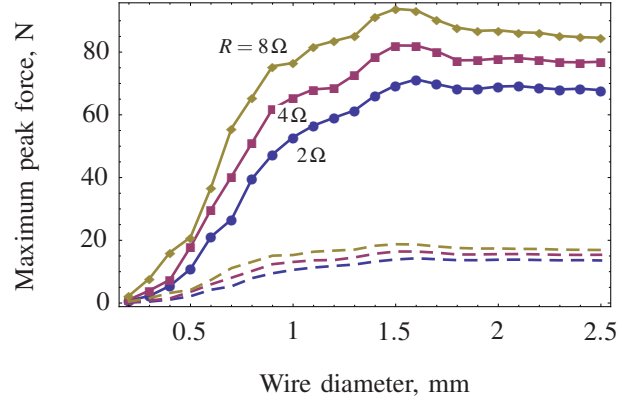


Fig. 11. Maximum peak force F_{\max} versus wire diameter calculated by multiplying the normalised maximum force by the maximum current rating for that wire diameter (Figures 10 and 9, resp.). Solid, labelled lines have a safety factor of 100%; dashed lines represent the same curves using a $S = 20\%$ safety factor; they exhibit the same shape with a proportionally lower peak amplitude.

As the maximum current rating data is applicable only for bare wire, a safety factor must be used for coils with many turns; a value of 20% is chosen for illustrative purposes here. Using this data, an estimate of the maximum peak force (after optimising the magnet and coil geometries individually) can be calculated for a range of wire diameters scaled according to their maximum current rating.

An upper estimate of the maximum force obtainable with a coil of certain wire diameter is found by multiplying the normalised maximum peak force by the maximum current rating, $F_{\max}(V_m, R, d_w, S) = \hat{F}_{\max}(V_m, R, d_w) \times I_{\max}(d_w) \times S$, using a safety factor S to account for unmodelled thermal effects. This produces the curves of maximum peak force shown in Figure 11, which each show a global maximum against wire diameter, although as the wire diameter increases the achievable peak force remains largely flat.

It is important to consider that these results can only be considered an upper limit on the possible forces achievable as the maximum operating temperature will be greatly limited

due to thermal effects. The shape of these curves, and hence the value of suitable wire diameter, is not affected by the safety factor chosen. Primarily, the curves in Figure 11 indicate that increasing the wire diameter is not effective past a certain point for the chosen constraints, being a maximum diameter of around 1 mm to 1.5 mm.

F. Trends in the optimisation results

It is interesting to consider the parameters chosen for the optimal values of magnet and coil ratios (Figure 12). As discussed earlier, due to quantisation errors in the calculation of radial turns, the optimal magnet and coil ratios are not smooth with wire diameter. Secondly, the accuracy of the numerical methods used to calculate these optimal values introduces numerical error into the results, and improving this accuracy is prohibitive in terms of calculation time.

Despite this, two broad characteristics can be seen. The magnet ratio is bound in most cases by around $1 \leq l_m/R_m \leq 2$. Secondly, as the wire diameter increases so does the coil ratio in an approximately linear relationship. The implication of this trend is that as the wire resistance per unit length decreases and the total length of wire increases (requiring more turns), it is advantageous to extend the length of the coil rather than to extend its outer radius. As shown in Figure 9, however, as the length of the coil exceeds the magnet length significantly, the normalised amount of force produced quickly decreases; driving the coil with a larger current is the only way to achieve parity with the shorter coils with smaller wire diameter.

G. Effects of magnet volume and coil resistance

Finally, while the results from Figure 11 indicate that increasing the coil resistance will lead to an increased maximum peak force for a given magnet volume, this increase leads to diminishing returns as the resistance increases past a certain point. This is shown in Figure 13 as a plot of maximum peak force versus coil resistance over a range of magnet volumes according to the function

$$F_{\max}(V_m, R) = \max_{d_w} \left\{ F_{\max}(V_m, R, d_w, S) \right\}, \quad (29)$$

using a safety factor of $S = 20\%$ to accommodate unmodelled thermal effects.

Qualitatively, this diminishing return in the maximum peak force can be explained by the fact that the larger the total coil resistance the longer the length of wire needed and the less compact the coil can be, resulting in a movement of the magnet field away from the permanent magnet. Therefore, despite the larger electrical energy input, this can only be achieved with a less efficient geometric design of the electromagnetic system. As added disadvantages to increasing the force in this way, the larger the resistance the greater the electrical power required to drive the coil at a certain current, the more windings required to construct the coil, and the greater the chance of thermal difficulties with the cooling of bulkier coils. Increasing the volume of the permanent magnet will generally be a more suitable approach to generating larger forces.

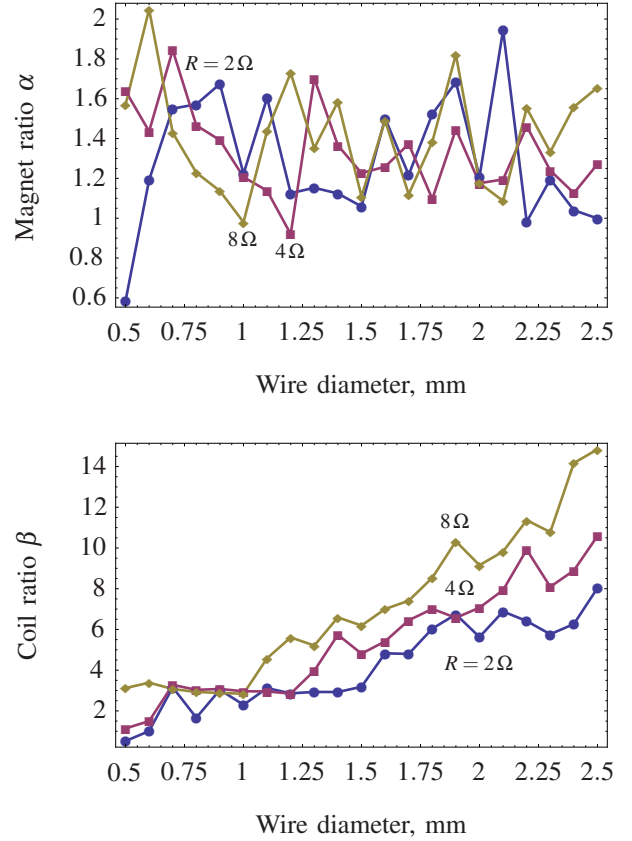


Fig. 12. Optimal values of magnet ratio α and coil ratio β corresponding to the results shown in Figures 9 and 11 for three resistance values.

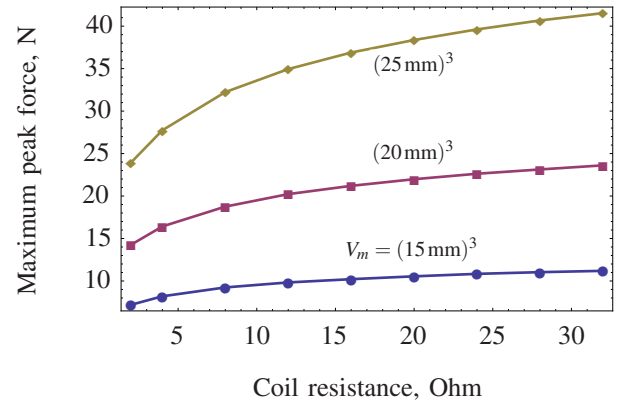


Fig. 13. Maximum peak force as a function of coil resistance for three magnet volumes, showing that an increase in coil resistance leads to diminishing returns in peak force. A safety factor of 20% has been applied to these results.

The overall outcome of this modelling is to conclude that after choosing a magnet volume and coil impedance, it is possible to optimise the force–displacement characteristic according to some cost function to choose the wire diameter, magnet shape, and number of coil turns. Designing a device to achieve a certain peak force, say, then requires simply choosing an appropriate magnet size and coil impedance, both of which depend on additional considerations including cost, availability of amplifier specifications, requirements for compact design, and so on.

V. CONCLUSION

In this paper we have summarised and compared the theory for analytically calculating the force generated between a thick coil of varying dimensions and a cylindrical permanent magnet with relative displacement in the axial direction. Despite the integral equation for this system being solved by other researchers almost entirely analytically, in some cases such a solution is computationally more expensive than numerical integration. An alternative solution using iteration over ‘shells’ of infinitely thin surface current densities is numerically cheaper again for coils with a relatively small number of radial turns.

This theory is suitable for optimising a wide range of actuator designs and in particular the general case of designing a magnetic actuator for peak force has been shown to reduce to choosing a coil impedance and magnet volume from which all geometric parameters are implicitly calculated. This design methodology can also be used to optimise the system parameters using other cost functions such as stroke length or linearity.

The numerical implementation of the equations in this paper are freely available and may be used to verify and extend this work.

APPENDIX

Corrected for a typographical error and rewritten slightly, the following is Babic et al.’s solution to equation (14) for calculating the force exerted on a permanent magnet by a thick coil. The sign of the result has been reversed over the original expression to ensure consistency with the results presented in this paper. Parameters are as described earlier in this publication.

$$F_{z_4} = \frac{NIB_r R_m^3}{6l_c [R_c - r_c]} \sum_{e_1, e_2, e_3}^{\{1, -1\}^3} [e_1 e_2 e_3 t f_{z_4}] \quad (30)$$

where

$$f_{z_4} = \psi_1 \sqrt{\rho m_7} + \frac{\pi \psi_2}{2|t|} + 6\psi_3, \quad (31a)$$

$$t = \frac{z + \frac{1}{2}e_1 l_m + \frac{1}{2}e_2 l_c}{R_m}, \quad (31b)$$

$$\rho = \frac{r_c + R_c + e_3 [R_c - r_c]}{2R_m}, \quad (31c)$$

$$m_7 = \frac{4\rho}{[\rho + 1]^2 + t^2}, \quad m_8 = \sqrt{t^2 + 1}, \quad (31d)$$

$$\psi_1 = K(m_7) \left[\frac{m_8 + 2}{m_8 + 1} [t^2 - 2] + \rho^2 + \rho + 2 - \frac{2}{\rho + 1} \right] - \frac{4\rho}{m_7} E(m_7) \quad (31e)$$

$$\psi_2 = \rho \operatorname{sgn}(\rho - 1) [\rho^2 - 3] \left[\Lambda_0(|\xi_1|, m_7) - 1 \right] + m_8 [t^2 - 2] \left[\Lambda_0(|\xi_2|, m_7) - 1 \right] + \operatorname{sgn}(\rho - m_8) \left[\Lambda_0(|\xi_3|, m_7) - 1 \right] \quad (31f)$$

$$\psi_3 = \int_0^{\pi/2} \operatorname{arcsinh} \left(\frac{\rho + \cos(2\varphi)}{\sqrt{\sin(2\varphi)^2 + t^2}} \right) d\varphi, \quad (31g)$$

$$\xi_1 = \operatorname{arcsin} \left(\frac{\rho - 1}{\rho + 1} \sqrt{\frac{1}{1 - m_7}} \right), \quad (31h)$$

$$\xi_2 = \operatorname{arcsin} \left(\frac{t}{m_8 + 1} \right), \quad (31i)$$

$$\xi_3 = \operatorname{arcsin} \left(\frac{t}{m_8 + 1} \sqrt{\frac{1}{1 - m_7}} \right), \quad (31j)$$

where Λ_0 is the Heuman Lambda function defined by

$$\Lambda_0(\phi, m) = \frac{2}{\pi} [F(\phi | 1 - m) [E(m) - K(m)] + E(\phi | 1 - m) K(m)], \quad (32)$$

and $\operatorname{sgn}(\cdot)$ represents the sign function

$$\operatorname{sgn}(x) = \begin{cases} -1 & x < 0, \\ 0 & x = 0, \\ +1 & x > 0. \end{cases} \quad (33)$$

When implementing equation (30), note that $t f_{z_4} = 0$ when $t = 0$ and the inner term f_{z_4} , which would otherwise contain a numerical singularity in this case, does not need to be evaluated.

REFERENCES

- [1] R. K. Cooper, V. K. Neil, and W. R. Woodruff, “Optimum permanent-magnet dimensions for repulsion applications,” *IEEE Transactions on Magnetics*, vol. MAG-9, no. 2, pp. 125–127, 1973.
- [2] E. P. Furlani, “A formula for the levitation force between magnetic disks,” *IEEE Transactions on Magnetics*, vol. 29, no. 6, pp. 4165–4169, Nov. 1993.
- [3] S. Babic and C. Akyel, “Magnetic force calculation between thin coaxial circular coils in air,” *IEEE Transactions on Magnetics*, vol. 44, no. 4, pp. 445–452, Apr. 2008.
- [4] R. Ravaut, G. Lemarquand, V. Lemarquand, S. I. Babic, and C. Akyel, “Mutual inductance and force exerted between thick coils,” *Progress In Electromagnetics Research*, vol. 102, pp. 367–380, 2010.
- [5] W. Robertson, B. Cazzolato, and A. Zander, “A simplified force equation for coaxial cylindrical magnets and thin coils,” *IEEE Transactions on Magnetics*, vol. 47, no. 8, pp. 2045–2049, 2011.
- [6] S. Babic, F. Sirois, C. Akyel, G. Lemarquand, V. Lemarquand, and R. Ravaut, “New formulas for mutual inductance and axial magnetic force between a thin wall solenoid and a thick circular coil of rectangular cross-section,” *IEEE Transactions on Magnetics*, vol. 47, no. 8, pp. 2034–2044, 2011.

- [7] A. Shiri and A. Shoulaie, "A new methodology for magnetic force calculations between planar spiral coils," *Progress In Electromagnetics Research*, vol. 95, pp. 39–57, 2009.
- [8] E. P. Furlani, *Permanent magnet and electromechanical devices*, I. Mayergoyz, Ed. Academic Press, 2001.
- [9] R. Ravaud, G. Lemarquand, V. Lemarquand, S. Babic, and C. Akyel, "Calculation of the magnetic field created by a thick coil," *Journal of Electromagnetic Waves and Applications*, vol. 24, no. 14, pp. 1405–1418, 7 2010.
- [10] H. W. Sams, *Handbook of Electronics Tables and Formulas*. Sams, 1986.